Understanding the key parameters for the rational design of layered oxide materials by composite sol-gel procedures

Samy Ould-Chikh, Nicolas Brodusch, Nathalie Crozet, Mehrdji Hemati, Loïc Rouleau

Understanding the key parameters for the rational design of layered oxide materials by composite sol–gel procedures

S. Ould-Chikh [a,*], N. Brodusch [a], N. Crozet [a], M. Hemati [b], L. Rouleau [a]

[a] IFP Energies nouvelles, Direction Catalyse et Séparation, Département Génie des Matériaux Divisés, BP-3, 69360 Solaize, France
[b] Laboratoire de Génie Chimique (LGC) de Toulouse, 4 allée Emile Monso-Bp 84234, 31432 Toulouse Cedex 04 France

Keywords:
Catalyst support
Layered oxide
Sol–gel
Granulation
Drying
Colloidal phenomena

A B S T R A C T

Previous works have well demonstrated that particle size of the filler used in layered oxide formulation is the first important parameter and must be decreased below 5 μm (Agrafiotis, 1999–2000 [10]). But once the particle size is set what are the next formulation parameters to highlight as critical? How do we improve cohesion and adhesion of the coatings?

To highlight the key parameters driving the quality of coating, a model layered oxide material was prepared inside a pan granulator. The model composite sol–gel formulation is based on boehmite nanoparticles (binder) and a monomodal two micrometer grain size gamma alumina (filler) which is applied onto alpha alumina beads substrate. The influences of the wetting method and relative amount of filler and binder were investigated. Extensive characterization and imaging of the layered materials (SEM, Cryo-SEM, EPMA, Washburn test, mechanical tests, Hg-porosimetry) were used in order to follow the microstructure evolution of coating during and at the end of drying. Several crack propagation schemes were observed and explained qualitatively.

Overall quality of coating is mainly related to the sol–gel transition of the binder. It defines if prior to shaping, the binder primer will be able to improve the coating adhesion and it defines also the nature and extent of damages that the coating undergoes during drying. The mechanical properties of layered oxide materials obtained using composite sol–gel formulation are definitely correlated with the binder gel shrinkage during drying.

1. Introduction

Layered oxide materials have often a hierarchical pore structure creating interesting features. Among them, the possibility to elaborate egg-shell catalysts with specific active sites restricted to the external material layer or in each material layers. The former strategy enables an overall enhancement of catalytic reactions subjected to diffusion limitations caused either by a low heat or a low mass transfer while the latter strategy constitutes an easy access to multifunctional materials. Thus, layered oxide materials have found an increased interest in very different application fields like exhaust depollution (NO_x reduction) [1], photocatalytic degradation of pollutants [2,3], CO_2 adsorption [4] and various refining reactions [5]. Industrial layered oxide materials are available as monoliths [6], beads [5], microreactors [7], or simply flat coated supports [6]. Several authors have composed comprehensive reviews of the coating methods which often involve CVD, PVD, electrophoretic deposition, and sol–gel technology [6–10]. The latter method is of a special interest as it exhibits the advantages of being simple and up-scalable, the ability to coat complex geometries all in using low temperature process and less complex equipment.

Sol–gel methods involve colloidal dispersion of oxides in water, which is then destabilized to produce a gel by subsequent drying, increase in ionic force, or neutralization of surface charges [11]. Dispersions are usually applied to supports by spray, dip or spin coating [12]. Despite its advantages, sol–gel technology presents strong limitations towards the maximum thickness (about 10 μm) reachable for a film [12]. This situation arises from large stresses induced during drying and/or densification. To address this issue, Barrow and Petroff [13] have developed sol–gel composite coating procedure to exceed this limitation i.e. when micrometric to submicrometric ceramic powders (filler) are dispersed in a ceramic matrix (binder) to produce a xerogel composite, a dramatic decrease of stresses are observed. The processing of larger size ceramic coatings then becomes possible. Furthermore, all metal oxide particles have also numerous surface hydroxyls creating oxo-bridge bonds between coating components during sintering, and thus improving coating anchoring and microstructure strengthening. Hence, this approach reveals to be flexible as it allows a wide variety of metal oxides able to be fitted to the formulation of suspensions.

Most of the published report deals with the preparation of thick coatings on different substrates by an extensive optimisation of the process and formulation parameters. It is rather proposed to rationalize the

* Corresponding author.
E-mail addresses: samy.ould-chikh@gmail.com (S. Ould-Chikh), mehrdji.hemati@ensiacet.fr (M. Hemati), loic.rouleau@ifpen.fr (L. Rouleau).

Table 1
Physical properties of the γ-Al_2O_3 powder (see Materials characterization for property definition).

	γ-Al_2O_3
d_{v10} (μm)	1
d_{v50} (μm)	2
d_{v90} (μm)	3
Skeletal density (g/mL)	3.28
Grain density (g/mL)	1.59
Bulk density (g/mL)	0.77
V_{meso} (mL/g)	0.35
d_{meso} (nm)	7
S_{BET} (m^2/g)	223

shaping of such coatings by a preliminary understanding of key parameters which determine its overall quality. We argue that – once the chemical compatibility between formulation components is established (at a molecular level) and the filler has a sufficient small particle size (<5 μm [10]) – phenomena setting the general coating adhesion and cohesion are all related to binder gelification. A model layered material made of alpha alumina millimetric spheres coated by a gamma alumina layer is chosen to highlight this assertion. For this purpose, a coating process is developed for a pan granulator where a dry γ-Al_2O_3 powder (filler) is added under a spraying of a boehmite sol (mineral binder) onto α-Al_2O_3 beads support. The relative proportion of binder and filler and the initial support wetting methods are investigated.

2. Materials and methods

The layered oxide materials are prepared by coating a γ-Al_2O_3 powder (filler) with a boehmite dispersion (binder) on the external surface of α-Al_2O_3 beads. The resultant materials are analysed using morphological, textural and mechanical characterization.

2.1. Raw materials

α-Al_2O_3 beads (Spheralite 512-Axens) sieved between 2.5 and 2.8 mm are used as a support. The nitrogen adsorption–desorption isotherm of Spheralite 512 is a type II according to the IUPAC classification. Spheralite 512 has a specific surface area of 8 m^2/g. The average pore diameter is 190 nm and porous volume is 0.48 mL/g. The mineral binder is made from a water dispersible boehmite (Pural SB3-Sasol). Primary particles are platelet-like morphology with an average crystallite size of 5 nm. A home-made mesoporous γ-Al_2O_3 powder is selected as filler. γ-Al_2O_3 grains are all spherical with a monomodal particle size distribution centred on 2 μm (Supplementary data, Fig. S1). Particle sizes, densities, and textural properties of γ-Al_2O_3 are grouped in Table 1.

2.2. Boehmite sols characterization

The water content W of a boehmite sol is defined as:

$$W = \frac{m_{H_2O}}{m_{AlOOH}} \quad (1)$$

where m_{H_2O} is the water mass (g), and m_{AlOOH} is the boehmite mass (g).

Table 2
Process parameters for investigating the effect of filler/binder ratio φ.

Shaping duration (min)	Filler flow rate (mL/min)	φ (vol.%)
26	0.52	13.3
45	0.30	8.9
65	0.20	7.2
85	0.16	6.1
100	0.14	5.4
116	0.12	4.8

The mineral binder is obtained by boehmite peptization with a water solution of nitric acid (HNO_3/AlOOH = 3.35 wt.% and W = 5). The boehmite dispersion is agitated during 2 h before enduring a centrifugation at 3800 *g* during 20 min to separate the non-peptized boehmite. Supernatant constitute the initial boehmite sol used as mineral binder. The latter boehmite sol is also sprayed in a diluted form with a higher water content (W = 32) to study its effect.

A dynamic light scattering instrument (Nanosizer ZS-Malvern) is used to determine the autocorrelation function of the backscattered intensity at 173° of an incident beam passing through boehmite sols. The effective diameter calculated from the cumulant analysis is used as a measurement of the mean particle size Z_{avg}. Particle size distribution – using a nonnegatively constrained least squares procedure (NNLS) – generally exhibits either a multimodal and/or a broad distribution for concentrated and diluted boehmite sols.

With "physical gels" like boehmite gel, sol–gel transition appears with an increase of medium ionic strength, surface charge neutralization, or a decrease of water content. As a unique boehmite sol formulation was used in this work either in its initial or diluted state, dependency of the sol–gel transition is restricted to only one parameter: the sol water content W. Usually when a sol–gel transition is triggered, a dramatic rise of the macroscopic viscosity is observed. This property is used to establish a phase diagram with a rheological method. Thus, 1 L of the diluted boehmite sol (W = 32) was divided into 100 mL volumes and placed into a ventilated oven at 50 °C. The choice of evaporation duration allows one to set the water content W of each sample. When a sample reaches the room temperature, it is placed into the air gap of a Couette rheometer (VT550-Haake). Samples are briefly sheared at 1200 s^{-1} and left static during 2 min. This preliminary procedure assures that each boehmite sol has received an identical stresses historical before characterization. Then a shear rate of 1200 s^{-1} is applied for 30 s while dynamic viscosity is recorded.

2.3. α-Al_2O_3 beads wetting

Monitoring capillary rise of the liquids (water and boehmite sols) inside the support is done with a Washburn test. α-Al_2O_3 beads are first grinded with a ball grinder and sieved between 150 and 250 μm. The resultant powder is placed into a 13.5 mm internal diameter and 100 mm length tube fitted with a permeable base. The tube is suspended above the studied surface liquid and on the beam of a precision balance (10^{-5} g) (Balance 3S-GBX) to record the mass evolution.

Some boehmite sols peptized with hydrochloric acid are also used to wet α-Al_2O_3 beads. As the X-ray fluorescence yield of chlorine is much higher than nitrogen, it allows one to use the chlorine counter ion as an X-ray marker. EPMA characterization (SX100-Cameca) is used to locate the chloride ions which have diffused within the porosity of α-Al_2O_3 beads. These samples are examined on polished cross section of beads embedded in a Bakelite resin. Five intensity profiles are recorded for aluminium and chlorine with an accelerating voltage of 15 kV and a backscattered electron detector.

Table 3
Volumetric fractions of pore ε_w filled by the liquid and coating attrition rates for coated α-Al_2O_3 beads obtained with a filler/binder ratio φ equal to 4.8 vol.% and a wetting method based on: water, a diluted boehmite sol, a concentrated boehmite sol.

Wetting liquid	W	ε_w (vol.%)	ξ (wt.%)
Water	+∞	92	100
Diluted sol	32	83	62
Concentrated sol	5	10	88

2.4. Coating procedure

Coating equipment is a laboratory pan granulator GRELBEX P30 equipped with a cylindrical conical bowl. Coating procedure starts with placing 100 g of beads in cascade state of flow at rotary speed of 40 rpm and 30° angle. Then surface wetting of α-Al_2O_3 beads is performed. The volumetric fraction of pore ε_w filled by the liquid is defined to help the analysis of the wetting period:

$$\varepsilon_w = 100 \cdot \frac{\dot{m}_s \cdot t_w}{V_p} \quad (2)$$

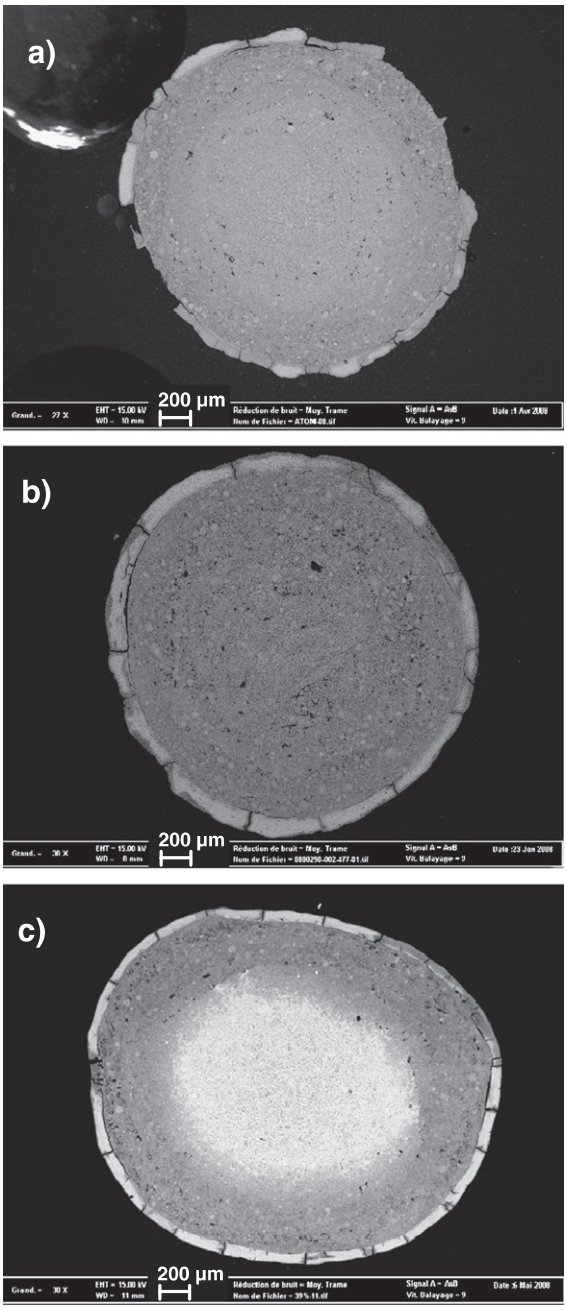

Fig. 1. SEM micrographs in polished section of coated α-Al_2O_3 beads obtained with a filler/binder ratio φ equal to 4.8 vol.% and a wetting method using: a) water, b) a diluted boehmite sol, and c) a concentrated boehmite sol.

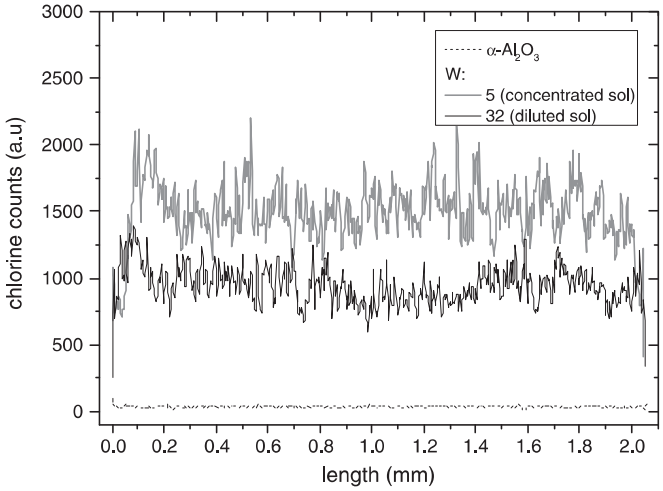

Fig. 2. Chlorine diametric distributions of α-Al_2O_3 beads wetted with a concentrated and diluted chlorhydric acid peptized boehmite sol measured by EPMA.

where $\dot{m}_s$ is the volumetric flow rate of liquid (mL/min), t_w is the wetting time (min), and V_p is the bead porous volume (mL). The wetting time t_w is set as the moment when the cascade state of flow is about to vanish. At this moment, α-Al_2O_3 beads have received on its surface a liquid film large enough for the further collection of filler particles. Coating thickness is chosen to be 80 µm and corresponds to the use of 13.6 mL of dry γ-Al_2O_3 powder, when considering the external surface of α-Al_2O_3 beads. γ-Al_2O_3 powder is continuously added under sol pulverisation with a volumetric flow rate $\dot{m}_s$ of 1 mL/min. The volumetric filler/binder ratio φ is defined as:

$$\phi = \frac{\rho_{AlOOH}}{\rho_{\gamma-Al_2O_3}} \frac{m_{\gamma-Al_2O_3}}{m_{AlOOH}} \quad (3)$$

where m_{AlOOH} is the total mass of sprayed binder (g), ρ_{AlOOH} is the binder grain density (g/mL) (calculated from a nitrogen adsorption isotherm on a boehmite xerogel), $\rho_{\gamma-Al_2O_3}$ is the filler bulk density (g/mL), and $m_{\gamma-Al_2O_3}$ is the mass of added filler (g).

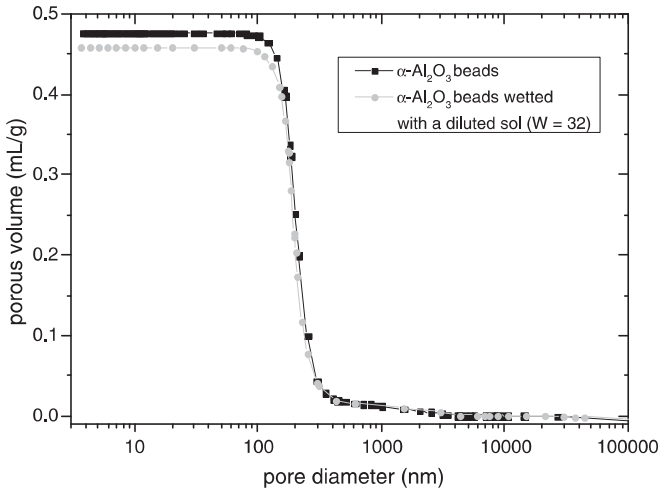

Fig. 3. Pore size distribution of α-Al_2O_3 beads and α-Al_2O_3 beads wetted with a diluted boehmite sol measured by mercury porosimetry.

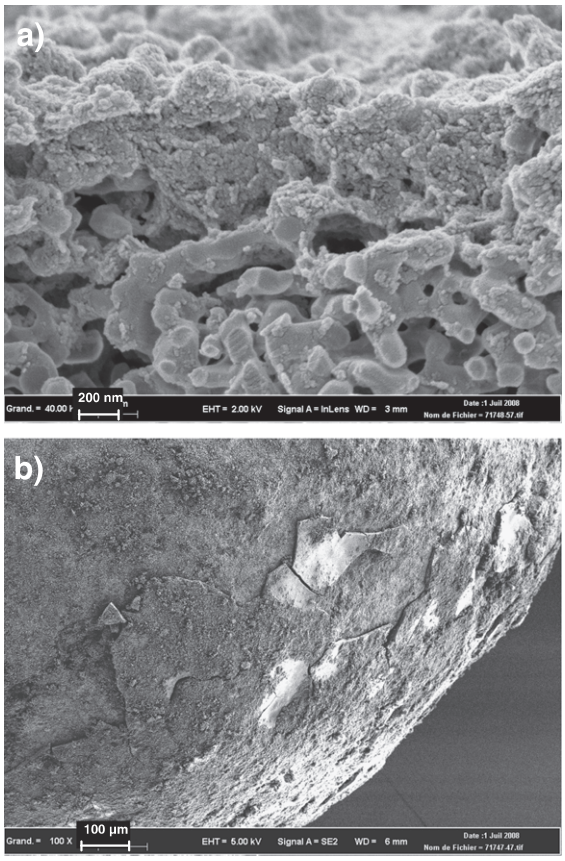

Fig. 4. SEM micrographs of a) a fractured α-Al_2O_3 bead wetted with a diluted boehmite sol and b) an α-Al_2O_3 bead surface wetted with a concentrated boehmite sol.

To highlight the effect of the wetting method, the filler/binder ratio is kept constant and equal to 4.8 vol.% and the used binder during the coating stage is based on a concentrated boehmite sol (W = 5). The wetting stage is then performed with three different liquids: water (W = +∞), a diluted sol (W = 32), and a concentrated sol (W = 5). The influence of the relative proportion of filler and binder is evaluated by setting the wetting and coating liquid to a diluted sol (W = 32)

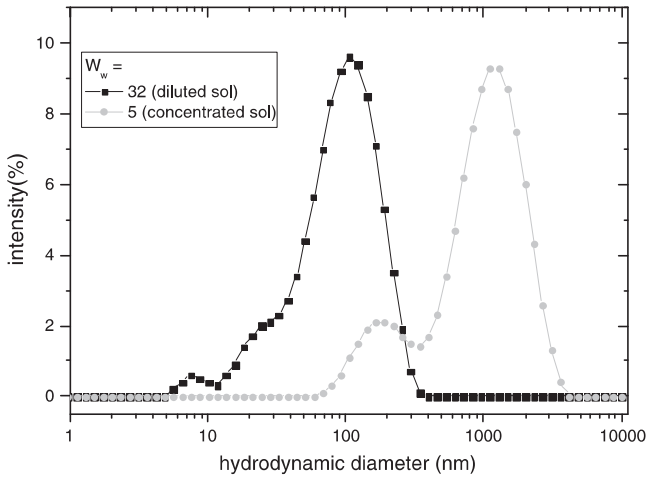

Fig. 5. Particle size distribution of a diluted (W = 32) and a concentrated (W = 5) boehmite sol measured by DLS.

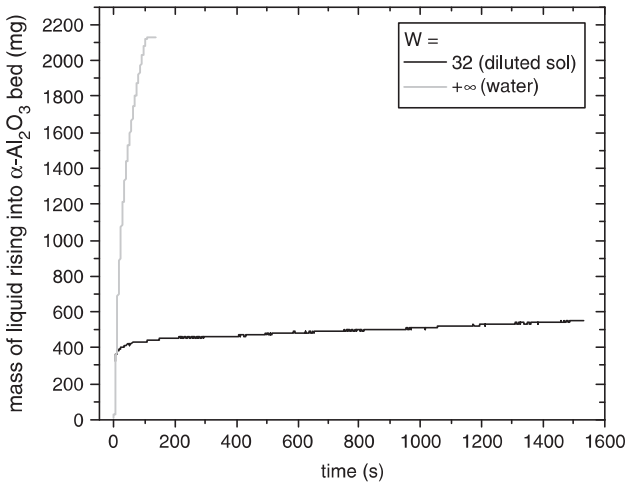

Fig. 6. Capillary ascent kinetics of water and a diluted boehmite sol into a grinded α-Al_2O_3 bed measured by Washburn test.

and adjusting the couple (procedure duration, filler flow rate) consistently (Table 2).

After adding the precursors, the coated beads are dried in a ventilated drying oven at 30 °C during 3 days. The coating rate d after drying is defined as follow:

$$d = \frac{m_d - m_{\alpha-Al_2O_3}}{m_{\alpha-Al_2O_3}} \quad (4)$$

where m_d is the mass of coated beads after drying, and $m_{\alpha-Al_2O_3}$ is the initial mass of α-Al_2O_3 beads. Efficiency e of coating process is evaluated and defined as follow:

$$e = \frac{d \times m_{\alpha-Al_2O_3}}{m_{AlOOH} + m_{\gamma-Al_2O_3}}. \quad (5)$$

2.5. Materials characterization

Pore size distribution of powder, beads and coated materials is determined by mercury porosimetry (Autopore 4-Micromeretics). Incertitude on porous volume is 0.01 mL/g. Specific surface areas are obtained by B.E.T. mathematical treatment on nitrogen physisorption

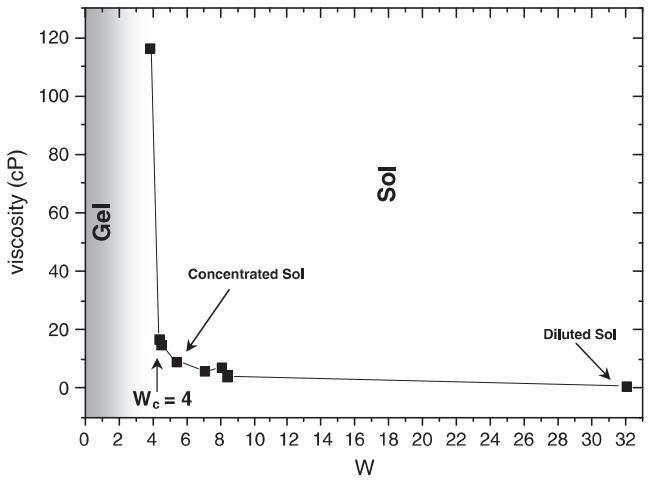

Fig. 7. Dynamic viscosity of the boehmite sol as a function of the water content W and phase diagram.

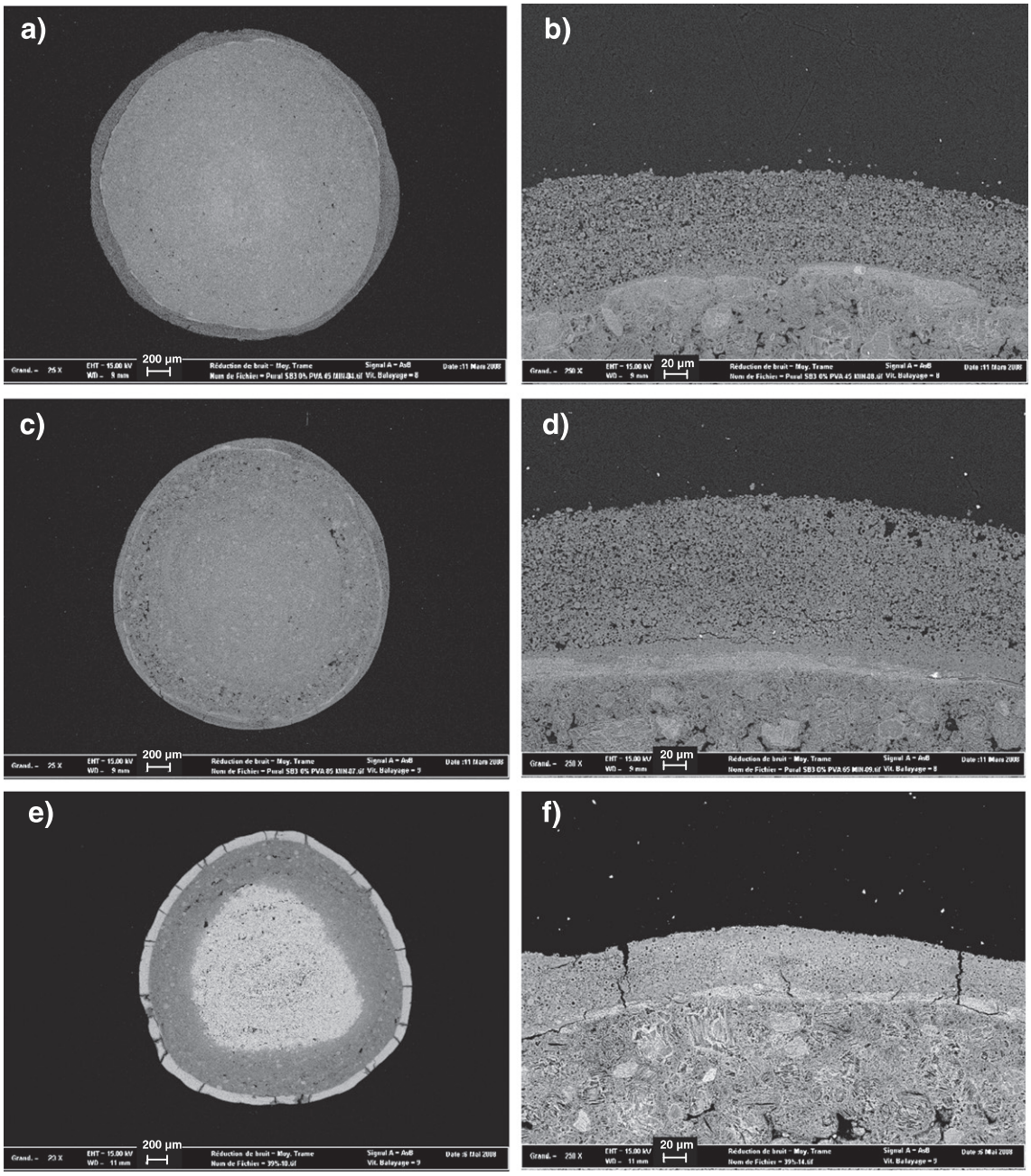

Fig. 8. SEM micrographs in polished section of coated α-Al_2O_3 beads using a 2 µm γ-Al_2O_3 particle size filler with a filler/binder ratio φ of 13.3 vol.% a) and b); 7.2 vol.% c) and d); 4.8 vol.% e) and f).

isotherms (ASAP 2420-Micromeretics). Skeletal densities of powders are measured by helium pycnometry (Accupyc-Micromeretics). Powder bulk density and grain density are calculated from pore size distribution and skeletal density. Particle size distribution of powders (d_{v10}, d_{v50} and d_{v90} such as 10 vol.%, 50 vol.% and 90 vol.% of particles are under that size, respectively) is measured by laser diffraction (Mastersizer 2000-Malvern). Morphology of boehmite nanoparticles is observed by TEM (JEM2100F-JEOL). Direct observation of raw materials and dried coated material are performed by SEM (Supra 40-Zeiss). Observations are done with an accelerating voltage of 5 kV with a secondary electron detector. Coated material microstructures are analysed on diameter polished section of coated beads embedded inside an epoxy resin. Observations are done with an accelerating voltage of 15 kV with a backscattered electron detector.

Cryogenic-SEM observations are used to follow the microstructure of coated materials during drying. Samples are maintained on a support within a small vice, before being inserted into a slush of nitrogen (60 K). Frozen coated materials are instantaneously mounted on an intermediate sample stage cooled by liquid nitrogen (CT1500-Oxford). Surface of coated materials are metalized by chromium and transferred to the liquid N_2 cooled SEM sample stage prior to surface observations. Thereafter, the samples are placed back in the cryogenic transfer system fitted with a knife which can be handled from outside. The samples are fractured and Cr-metalized prior to cross-sectional observations. All micrographs are captured with an accelerating voltage of 3 kV and a secondary electron detector. Characterized coating formulations by Cryo-SEM are those comprising the largest amount of sprayed binder in order to highlight mechanisms altering the coating. Coated α-Al_2O_3

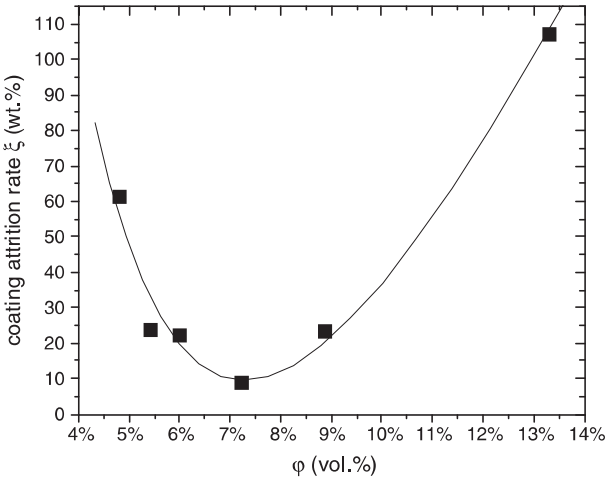

Fig. 9. Coating attrition rate of coated α-Al_2O_3 beads using a 2 μm γ-Al_2O_3 particle size filler given as a function of filler/binder ratio φ.

beads are observed immediately after shaping, 2 h drying at 30 °C and 3 days drying at 30 °C.

2.6. Mechanical characterization

Before characterization, dried coated materials are sintered in a muffle furnace at 600 °C for 2 h in air using a heating rate of 3 °C/min. During that stage, boehmite particles lose its structural water and are converted by a topotactic transformation into γ-Al_2O_3 [14]. A final coating rate c is defined as the coating mass is decreased:

$$c = \frac{m_c - m_{\alpha-Al_2O_3}}{m_{\alpha-Al_2O_3}} \quad 6$$

where m_c is the mass of coated material after calcination.

The choice of a mechanical characterization procedure for coated spherical material is described in details elsewhere [15]. Mechanical characterization is performed inside a drum attrition test. The device is composed of a cylinder with an internal diameter of 40 mm and a height of 80 mm closed at its ends by two stoppers screwed over a Teflon shirt. The drum is rotated during 136 min using 25 g of coated beads. At the end of each test, samples are sieved on 2 mm sieve during 1 min on a sieving machine Retsch AS-200 with the weakest intensity. The oversized and undersized particles are called respectively "mother particles" and "cuttings". Attrition rate of the coating ξ is defined as follow:

$$\xi = \frac{m_c - m_m}{c \times m_{\alpha-Al_2O_3}} \quad 7$$

where m_m is the mass of mother particles.

3. Results and discussion

3.1. α-Al_2O_3 beads wetting

At the end of the wetting stage, the pore volume of α-Al_2O_3 beads is almost filled by water ($\varepsilon_w = 92$ vol.%) (Table 3). With a diluted boehmite sol, the fraction of the porosity filled by liquid is slightly reduced. When using a larger concentration of boehmite, the filled pore volume radically drops (from $\varepsilon_w = 83$ vol.% to $\varepsilon_w = 10$ vol.%) (Table 3).

Coatings are segmented in several blocks for all wetting methods (Fig. 1). The damages looks stronger for a water wetting method as some pieces of coating are missing (Fig. 1a). Hence, coating adhesion is very weak for a water wetting compared to a boehmite sol wetting (Fig. 1b and c). Those observations are in accordance with measured attrition rate which shows that the whole coating is removed when a water wetting method is used (Table 3). Mechanical strength of coatings is enhanced when a boehmite sol is used to wet the α-Al_2O_3 beads, especially with a diluted boehmite sol (Table 3).

To better understand how the deposition of a boehmite primer enhances the coating adhesion and why using a diluted sol give better results, a new wetting operation (without shaping) was performed with a boehmite sol peptized with chlorhydric acid (instead of nitric acid). EPMA chlorine profile indicates a uniform distribution of chlorine into the beads for both boehmite sol concentrations (Fig. 2). Thus, water from boehmite sol is able to diffuse through alpha alumina beads.

As the longest dimension of boehmite platelet is 20 nm and the pore size distribution of α-Al_2O_3 beads is centred on 190 nm, one should also expect an extensive penetration of single boehmite particles into the support and thereby a modification of the initial porosity of the beads. But pore size distribution of initial and impregnated beads remains almost identical (Fig. 3). Despite the large amount of sprayed boehmite sol, the pore opening of α-Al_2O_3 beads remains available and boehmite particles do not coat the internal porosity of α-Al_2O_3 beads. Only a slight decrease of the porous volume is observed. It might indicate that deposited boehmite is generating a small pore size that mercury porosimetry measurement cannot reach within the range of applied pressure.

The boehmite deposit was located by SEM. With the diluted sol, boehmite platelets slightly penetrate into the support (500 nm to 3 μm depth) (Fig. 4a). The building of a composite interface made of boehmite/alpha alumina prior to shaping further enhances the coating anchoring. When sol concentration is increased, the boehmite particles remain on surface beads and form a thin crackled xerogel film with a low adhesion (Fig. 4b). This clarifies why a wetting method with a diluted sol improves mechanical strength compared to a concentrated sol.

If single boehmite particles are small enough to fit into alpha alumina pores, what about aggregate of particles? Particle size distribution of boehmite sols shows a large aggregation of boehmite elementary particles increasing with boehmite concentration (Fig. 5). For the concentrated sol, the mean aggregate size is so large – $Z_{avg} = 520$ nm compared to the 190 nm pore diameter of α-Al_2O_3 beads – that it explains by itself why all the boehmite particles are deposited on the surface of α-Al_2O_3 beads. For the diluted sol, aggregate is smaller ($Z_{avg} = 68$ nm) and thus it does not explain why only a small periphery of α-Al_2O_3 beads is penetrated by boehmite particles.

Capillary suction kinetics of water and diluted boehmite sol through a grinded α-Al_2O_3 bed are presented on Fig. 6. Water rise up quickly into the α-Al_2O_3 bed, while the diluted boehmite sol ascends initially with an identical rate, but a rate breakdown occurs shortly afterward. When the capillary tube was later opened, a boehmite gel plug was observed at the bottom setting up a diffusion barrier.

The wetting of α-Al_2O_3 beads with a boehmite sol is a dynamic phenomenon. Indeed, as water diffuses much faster than boehmite aggregates into α-Al_2O_3 pores (because of the Van der Waals attractive interactions between solids), the boehmite sol is progressively concentrated on the surface of α-Al_2O_3 beads. The formulated boehmite sol has a gel point characterized by a critical gelation point at W_c equal to 4 (Fig. 7) [16]. The quantity that drives the sol–gel transition is given by the "gelification distance" defined as $\Delta W = |W - W_c|$. While gelification distance progressively approaches zero upon water capillary suction, aggregation of boehmite particles becomes stronger while macroscopic viscosity rises up. The last stage of this process is the appearance of the sol–gel transition which freezes locally the sol on the surface of α-Al_2O_3 beads. This process explains why a smaller aggregate size is not a sufficient condition to allow a complete diffusion of boehmite particles into α-Al_2O_3 beads and why such a small fraction of the beads porosity was filled by wetting liquid when using a concentrated sol ($\varepsilon_w = 10$ vol.%). Capillary suction of water shifts the state of a sol deposited on a porous substrate from a diluted to a concentrated state, and eventually to a gel.

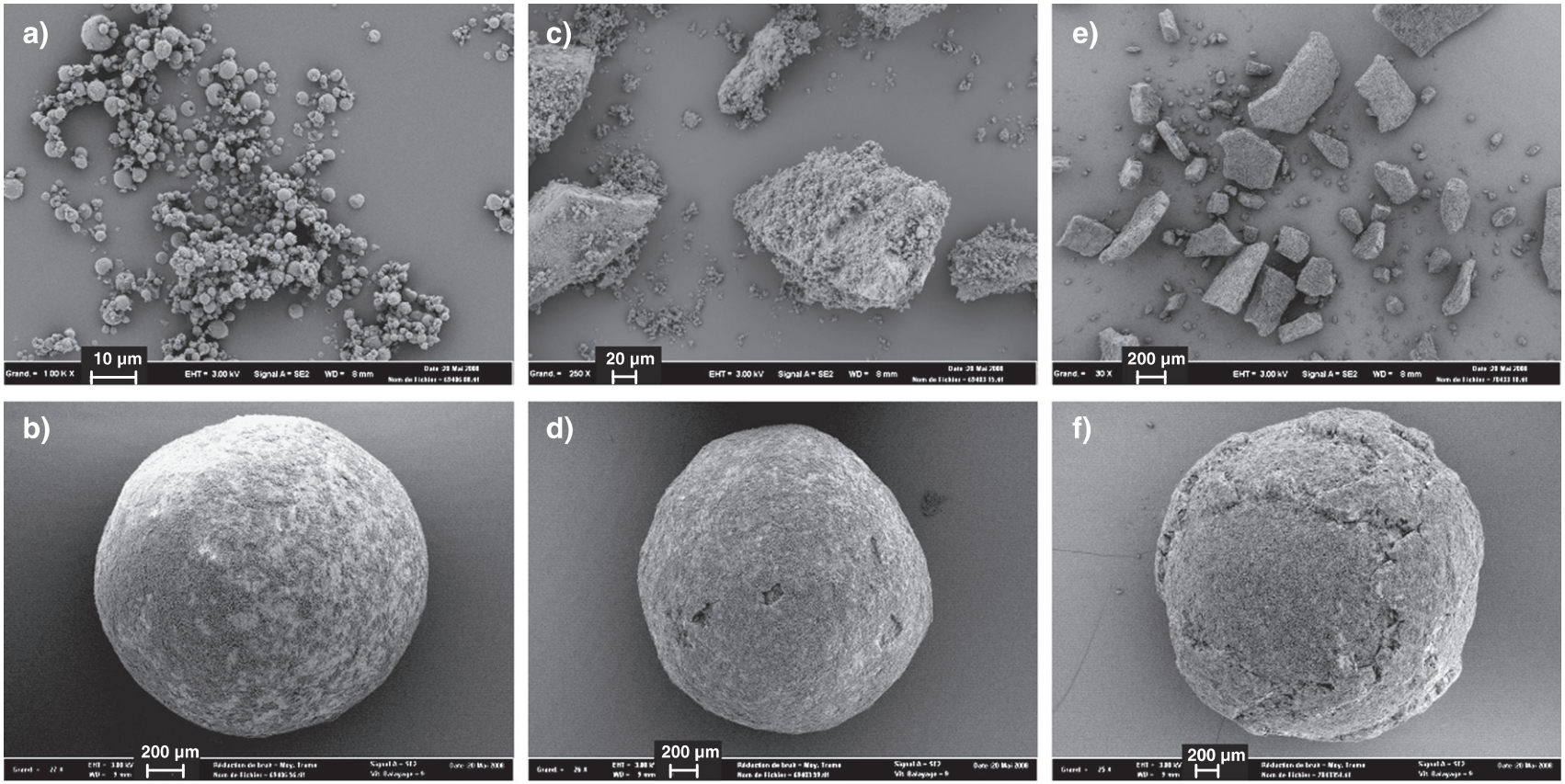

Fig. 10. SEM micrographs of particles generated during a drum attrition test of coated α-Al_2O_3 beads. Cuttings and mother particles for a filler/binder ratio φ equal to 13.3 vol.% a) and b); 7.2 vol.% c) and d); 4.8 vol.% e) and f).

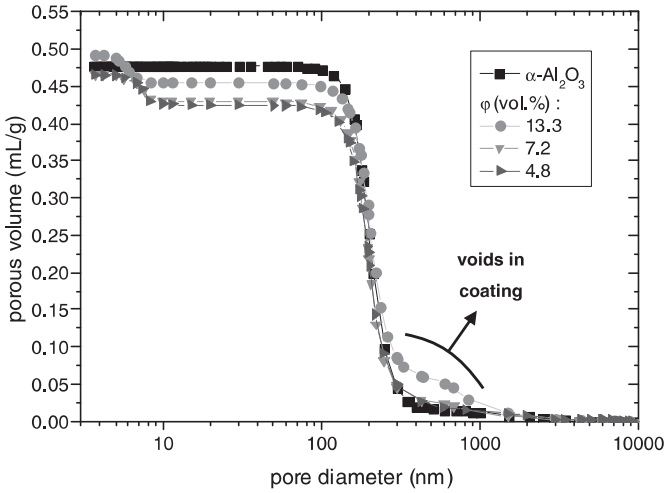

Fig. 11. Pore size distributions of uncoated and coated α-Al_2O_3 beads using on a 2 μm γ-Al_2O_3 particle size filler and three filler/binder ratios.

3.2. Filler/binder ratio φ

Efficiencies above 95% are obtained for all coating operations. SEM observations show a granular microstructure for all coatings with a homogeneous 80 μm thickness (Fig. 8) while coating attrition rate presents a minimum with φ equal to 7.2 vol.% (Fig. 9).

For the highest filler/binder ratios, coating is macroporous because of insufficient boehmite content between gamma alumina grains. No segmentation of the coating is observed for the highest filler/binder ratios (Fig. 8a and b). Cuttings obtained after drum attrition test are mostly made of single grain of filler (Fig. 10a). Observations of mother particles surface indicate that almost all of the deposited coating is peeled off as surface of α-Al_2O_3 beads is clearly visible (Fig. 10b). Hence, the lack of binder is responsible for the reduced mechanical strength. At filler/binder ratio giving the best mechanical strength ($\varphi = 7.2$ vol.%), a slight segmentation phenomenon takes place and coatings still comprise some large voids (Fig. 8c and d). Cuttings obtained after drum attrition test are composed of elementary grains of filler and agglomerated filler grains into blocks (Fig. 10c). Observations of mother particles surface indicate that most of coating withstood the drum attrition test as only small pieces of coating are missing (Fig. 10d). For the lowest filler/binder ratios, coatings are increasingly compact but segmentation phenomenon consequently deepens and ultimately lessens the mechanical strength (Fig. 8e and f). Cuttings obtained after drum attrition test are large blocks of coating (Fig. 10e), while remaining mother particles indicate that about half of the deposited coating is missing (Fig. 10f). The coating attrition rate minimum observed for $\varphi = 7.2$ vol.% match up a compromise between coating densification and segmentation.

Pore size distribution of coated materials exhibits a mesoporous volume of 0.04 mL/g to 0.05 mL/g generated by the coating with an average diameter of 6 nm and a macroporous volume generated by α-Al_2O_3 beads (Fig. 11 and Table 4). For the highest filler/binder ratio, pore size distribution presents also a significant porous volume between 1000 nm and 300 nm similar to the size of voids generated by a powder bed of filler. Assuming that porous volume of coated materials is a linear function of porous volume of beads and coating, macroporous volume of coating $V_{coating}$ is calculated with Eq. (8):

$$V_{coating} = \frac{V_{coated\ \alpha-Al_2O_3} \times (1+d) - V_{\alpha-Al_2O_3}}{d} \quad 8$$

where $V_{\alpha-Al_2O_3}$ and $V_{coated\ \alpha-Al_2O_3}$ are the respective measured macroporous volume ($50–10^5$ nm) of α-Al_2O_3 beads and coated α-Al_2O_3 beads. As macroporous coating volume decreases with lowering filler/binder ratio, it further supports the conclusion that coating densification is improved for the highest boehmite contents in coating (Table 4).

Table 4
Mesoporous volumes of coated α-Al_2O_3 beads and macroporous volumes of coating as a function of filler/binder ratio.

φ (vol.%)	V_{meso} (mL/g)	$V_{coating}$ (mL/g)
13.3	0.04	0.3
8.9	0.04	0.3
7.2	0.04	0.1
6.1	0.05	0.1
5.4	0.04	0.1
4.8	0.05	0.1

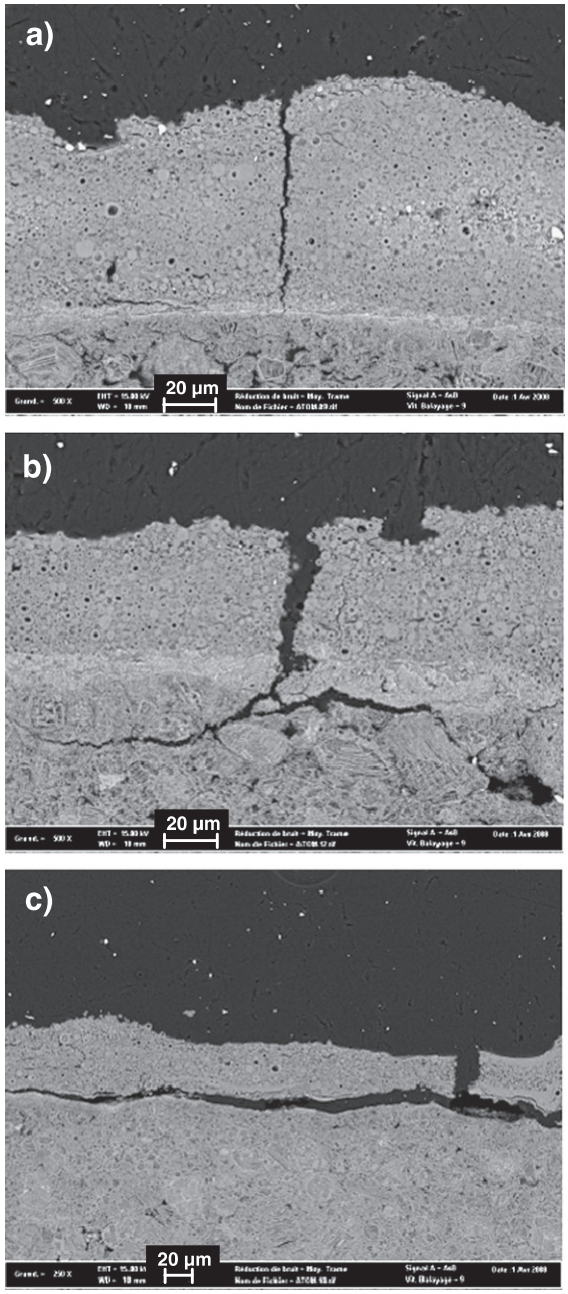

Fig. 12. SEM micrographs in polished section of cracks initiated on coating surface, a) stopped at the interface, b) propagated inside the bead, and c) and propagated at the interface with a filler/binder ratio φ equal to 4.8 vol.%.

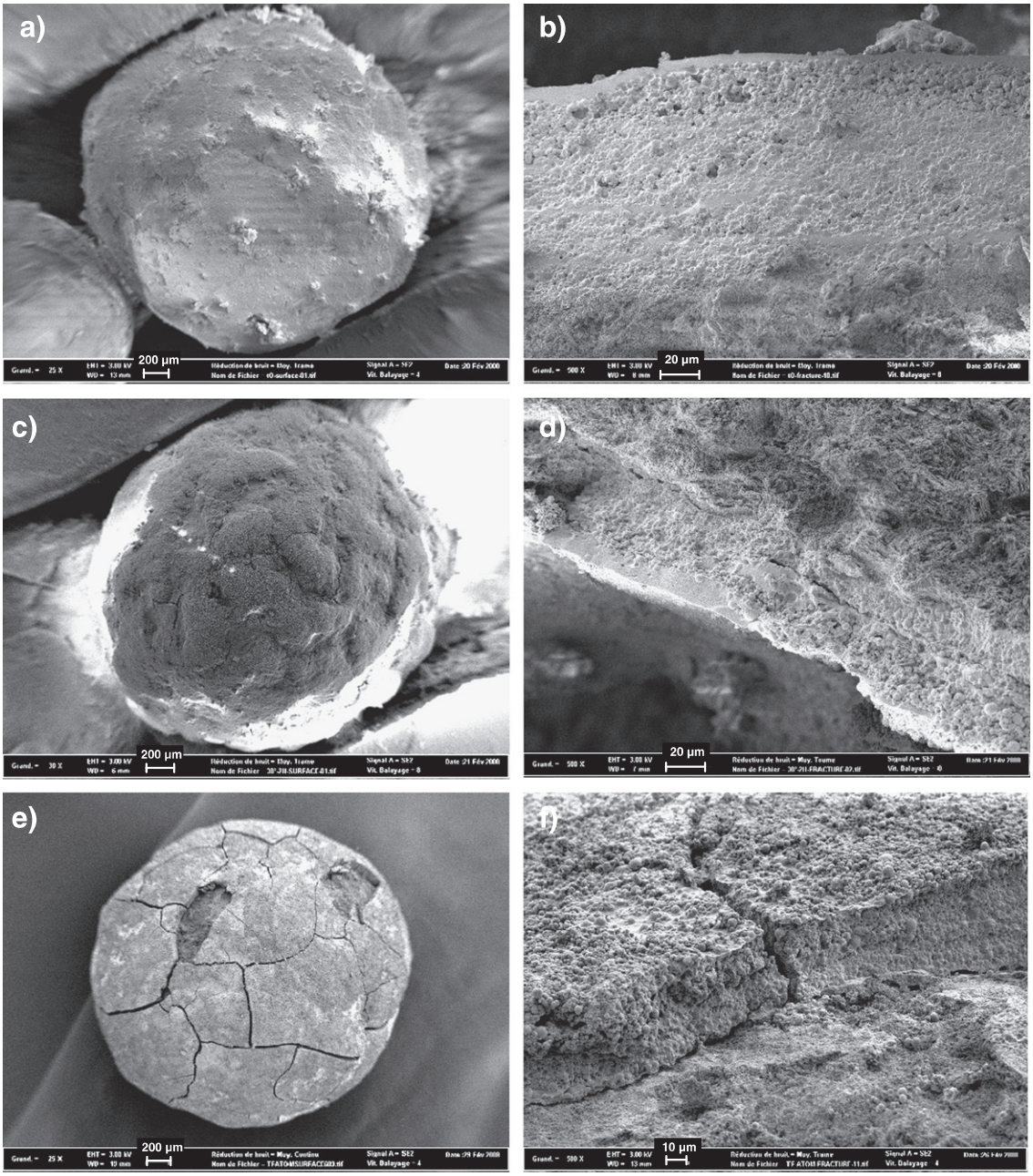

Fig. 13. Cryo-SEM and SEM micrographs of coated α-Al_2O_3 using a 2 µm γ-Al_2O_3 particle size filler and a filler/binder ratio φ equal to 4.8 vol.% after: a) and b) shaping; c) and d) 2 h drying at 30 °C; e) and f) 3 days drying at 30 °C.

However, large sprayed amount of boehmite leads in addition to the creation of new types of microstructural defects. These appear on SEM micrographs mainly as macro-cracks which seem to be initiated on coatings surface. They may propagate at the interface and stop (Fig. 12a), penetrate into the support (Fig. 12b), or either propagate at the coating/bead interface (Fig. 12c).

Cryo-SEM observations right after shaping of coated α-Al_2O_3 beads with the largest amount of sprayed boehmite did not present any surface crack (Fig. 13a). Observations on fractured samples show that boehmite is rather well distributed through the coating (Fig. 13b). After a 2 h drying at 30 °C, the coating is separated in several rounded contracting blocks (Fig. 13c). No significant change in coating microstructure is observed (Fig. 13d). At the end of the drying, coatings are subjected to a strong segmentation. Some pieces of coating are even missing (Fig. 13e). Segmentation and interfacial cracks are easily observed (Fig. 13f).

At the end of the shaping procedure, α-Al_2O_3 beads are coated by a layer of spherical γ-Al_2O_3 grains bonded together by capillary pressure and liquid surface tension forces. As drying progress, gelification distance ΔW reaches zero and boehmite sol makes its final sol–gel transition between γ-Al_2O_3 grains. Boehmite gels obtained from Pural SB3 boehmite are known to undergo large isotrope shrinkage during drying (up to 60 vol.%) [17]. In the present case, the wet coating is considered as a boehmite gel matrix in which are embedded γ-Al_2O_3 grains. The composite gel is a continuous field deposited on α-Al_2O_3 beads surface (Fig. 14a). Upon drying, gel shrinkage operates (Fig. 14b) and causes a multiple segmentation of the coating (Fig. 14c). Pourcel has proved that at the beginning of drying, water content into a boehmite gel

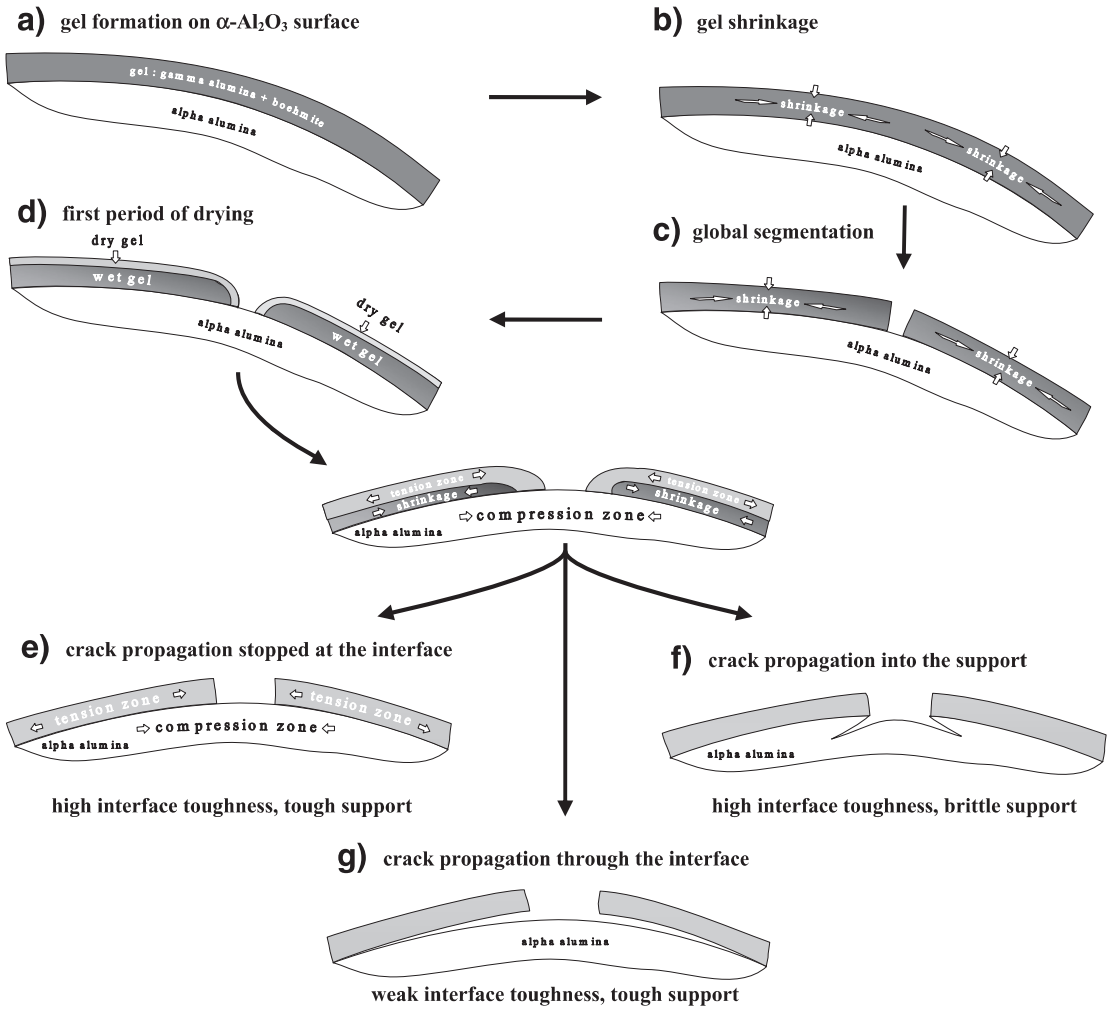

Fig. 14. Scheme of damaging mechanisms of α-Al_2O_3 beads coated by a composite gel during drying.

surface is lower than the boehmite gel core: surface contracts whereas the core keeps appreciably its dimensions [17]. This deformation state causes a setting in traction of the surface compensated by a compression of the gel core. The second period of drying begins when the material surface shrinkage does not evolve/move anymore. Surface dimensions are then fixed whereas the gel core continues to contract. Doing so, the gel core applies a compressive force to surface and surface a traction effort to the core: it is the stress inversion. This phenomenon might explain the rounded shaped block of composite gel observed during drying (Figs. 13c, 14d). The third period corresponds to the end of drying where water gradients are negligible.

For the simple case of a pure boehmite gel which is non-supported, stresses tend towards zero and the material regains its initial shape but on a reduced scale. However, with a supported composite gel, traction forces that α-Al_2O_3 beads apply in response to the general coating shrinkage are expected to leave residual tension stresses in the coating. Previous results support that intensity of stresses is greater when the amount of boehmite introduced into the coating increases because of larger gel shrinkage. The latter stresses may lead to crack propagation as described in details by Hutchinson and Suo [18]. Crack propagation schemes are determined by the relative tenacity and Young's modulus of support, interface, and coating when two brittle materials are contacted [18,19]. Schematically, a high interface and support toughness cause crack propagation to stop at the interface (Fig. 14e), high interface toughness and a brittle support cause crack to propagate into the support (Fig. 14f), and a weak interface and high support toughness cause crack to propagate along the interface (Fig. 14g). Occurrence of all crack propagation schemes (Fig. 12) indicates these parameters were of the same magnitude order.

4. Conclusion

A model layered oxide material based on a γ-Al_2O_3 filler, a boehmite binder, and a α-Al_2O_3 spherical substrate was shaped in a pan granulator to highlight the key parameters defining the overall quality of coatings when composite sol–gel formulations are used:

- The deposition of a binder primer is essential to provide adhesion to the coating.
- Adhesion is further enhanced when a porous substrate allows the binder to penetrate enough to create a strong composite interface.
- The latter penetration depth is controlled by the sol–gel transition of the binder sol and the capillary suction into the porous substrate.
- Relative amount of filler and binder controls the type of damage that coating meets during drying:
  - o Low amount of binder: coatings are highly porous and weak due to the lack of binder.
  - o High amount of binder: coatings are compact but segmented in several pieces due to the gel shrinkage of the binder.

- Propagation of cracks in coating with large amount of binder depends on:
  - o The relative mechanical properties of coating, interface, and substrate.
  - o The stresses occurring during drying of which intensity is related to the shrinkage of the gel.

The gel point of a sol sets the total volume of water to evaporate from the initial hydrogel and thus defines the total shrinkage at the end of dying [17]. As the gel point is known to be strongly dependent of size and morphology of binder particles, ionic strength, and presence of additives, a wide field is opened to finely tune adapted mineral binders. The latter outlook is expected to allow one reducing the gel shrinkage during drying and thus succeeding in shaping perfect coating.

This study has constituted an outstanding base to design industrial layered supports offering an exceptional cohesion and adhesion [20] and an adapted porosity for the catalytic selective hydrogenation of olefins as a first application [21,22].

Supplementary data to this article can be found online at http://dx.doi.org/10.1016/j.powtec.2012.11.010.

References

[1] M.V. Twigg, Catalytic control of emissions from cars, Catalysis Today 163 (2011) 33–41.

[2] D.H. Chen, K. Li, R. Yuan, Photocatalytic Coating on Road Pavements/Structures for NO_x Abatement, ANNUAL Project Report Submitted to Houston Advanced Research Center and Office of Air Quality Planning and Standards U.S. Environmental Protection Agency, 2007.

[3] M. Guarino, A. Costaa, M. Porroa, Photocatalytic TiO_2 coating to reduce ammonia and greenhouse gases concentration and emission from animal husbandries, Bioresource Technology 99 (7) (2008) 2650–2658.

[4] S. Kimura, M. Adachi, R. Noda, M. Horion, Particle design and evaluation of dry CO_2 recovery sorbent with a liquid holding capability, Chemical Engineering Science 60 (2005) 4061–4071.

[5] R.H. Jensen, J. Bricker, Q. Chen, M. Tatsushima, K. Kikuchi, M. Takayama, K. Hara, Layered Catalyst Composition and Processes for Preparing and Using the Composition, WO0241990A1, UOP, 2002.;
I.A. Cody, M.M. Hafez, D.N. Zinkie, Catalyst Comprising Thin Shell of Catalytically Active Material Bonded onto an Inert Core, US 5,200,382, Exxon, 1993.;
J.F. Lindsley, Hydrotreating Catalyst Support having Dual Pore Structure, US 4,465,789, American Cyanamid Company, 1984.

[6] A. Cybulski, J.A. Moulijn, Structured catalysts and reactors, in: Chemical Industries, vol. 71, Marcel Dekker, New York, 1998;
P. Avila, M. Montes, E.E. Miro, Monolithic reactors for environmental applications: a review on preparation technologies, Chemical Engineering Journal 109 (2005) 11–36;
T.A. Nijhuis, A.E.W. Beers, T. Vergunst, I. Hoek, F. Kapteijn, J.A. Moulijn, Preparation of monolithic catalysts, Catalysis Reviews 43 (4) (2001) 345–380.

[7] L. Kiwi-Minsker, A. Renken, Microstructured reactors for catalytic reactions, Catalysis Today 110 (2005) 2–14;
L. Kiwi-Minsker, A. Renken, Chapter 2 — microstructured catalytic reactors, Advances in Catalysis 53 (2010).

[8] V. Meille, Review on methods to deposit catalysts on structured surfaces, Applied Catalysis A: General 315 (2006) 1–17.

[9] D.K. Ward, E.I. KO, Preparing catalytic materials by the sol–gel method, Industrial and Engineering Chemistry Research 34 (1996) 421–433.

[10] A. Stefanescu, A.C. Van Veen, C. Mirodatos, J.C. Beziat, E. Duval-Brunel, Wall coating optimization for microchannel reactors, Catalysis Today 125 (2007) 16–23;
P. Pfeifer, K. Schubert, G. Emig, Preparation of copper catalyst washcoats for methanol steam reforming in microchannels based on nanoparticles, Applied Catalysis A: General 286 (2005) 175–185;
C. Agrafiotis, A. Tsetsekou, The effect of powder characteristics on washcoat quality. Part I: alumina washcoats, Journal of the European Ceramic Society 20 (2000) 815–824;
C. Agrafiotis, A. Tsetsekou, A. Ekonomakou, The effect of particle size on the adhesion properties of oxide washcoats on cordierite honeycombs, Journal of Materials Science Letters 18 (1999) 1421–1424.

[11] L.J. Gauckler, Th. Graule, F. Baader, Ceramic forming using enzyme catalysed reactions, Materials Chemistry and Physics 61 (1999) 78–102.

[12] C.J. Brinker, G.W. Scherer, Sol–gel Science: The Physics and Chemistry of Sol–gel Processing, Academic Press, 1990.

[13] D.A. Barrow, T.E. Petroff, M. Sayer, Method for Producing Thick Ceramic Films by a Sol Gel Coating Process, WO9629447, Queen's University at Kingston, 1996.;
D.A. Barrow, T.E. Petroff, M. Sayer, Thick ceramic coatings using a sol–gel based ceramic–ceramic 0–3 composite, Surface and Coatings Technology 76–77 (1995) 113–118.

[14] In: F. Schüth, K.S.W. Sing, J. Weitkamp (Eds.), Handbook of Porous Solids, vol. 3, Wiley-VCH, 2002, (Chapter 4.7.2);
S.J. Wilson, A kinetic study of the system γ-AlOOH/Al_2O_3, Journal of Solid State Chemistry 34 (1980) 315–322.

[15] S. Ould-Chikh, B. Celse, M. Hemati, L. Rouleau, Methodology of mechanical characterization of coated spherical materials, Powder Technology 190 (2009) 19–24.

[16] M.J. Gieselmann, M.A. Anderson, Effect of ionic strength on boehmite hydrogel formation, Journal of the American Ceramic Society 72 (6) (1989) 980–985.

[17] F. Pourcel, W. Jomaa, J.R. Puiggali, L. Rouleau, Criterion for crack initiation during drying: alumina porous ceramic strength improvement, Powder Technology 172 (2007) 120–127.

[18] J.W. Hutchinson, Z. Suo, Mixed mode cracking in layered materials, Advances in Applied Ceramics 29 (1992) 63–191.

[19] E.G. Evans, M.D. Drory, M.S. Hu, The cracking of thin films, Journal of Materials Research 3 (1988) 1043–1049.

[20] S. Ould-Chikh, Elaboration, mise en forme, et résistance mécanique de bi-matériaux sphériques application en catalyse, Ph.D. thesis, University of Lyon, France, 2008.

[21] S. Ould-Chikh, S. Pavan, A. Fecant, E. Trela, C. Verdon, A. Gallard, N. Crozet, J.-L. Loubet, M. Hemati, L. Rouleau, Hierarchical porous catalyst support: shaping, mechanical strength and catalytic performances, Studies in Surface Science and Catalysis 175 (2010) 193–200.

[22] S. Ould-Chikh, A. Fecant, L. Rouleau, L. Fischer, M. Hemati, Method of Preparing a Core–shell Material having Good Mechanical Strength, WO10020717A2, IFPEN, 2010.